

Oxygen transfer across the air–water interface by natural convection in lakes

S. Geoffrey Schladow

Department of Civil and Environmental Engineering, University of California, Davis, California 95616

*Minhee Lee*¹

Department of Civil and Environmental Engineering, University of California, Davis, California 95616

Bernhard E. Hürzeler

Department of Civil and Environmental Engineering, University of California, Davis, California 95616

Peter B. Kelly

Department of Chemistry, University of California, Davis, California 95616

Abstract

Oxygen transfer associated with natural convection in lakes and reservoirs was examined in a series of laboratory experiments. A thin, cool surface water layer (2–3 mm in thickness) was formed by chilling the air overlying a tank of surface area 0.6 m² and depth 0.6 m. The surface water layer became gravitationally unstable, resulting in the formation of negatively buoyant thermal plumes, which penetrated through the total depth of the water column. The spatial distribution of oxygen concentration at the air–water interface in the tank was visualized using a fluorescence imaging technique to quantify the oxygen transfer driven by only natural convection. Pyrenebutyric acid (PBA) at a concentration of 3.0×10^{-6} mole L⁻¹ was used as the fluorophore, and the quenching of the fluorescence by oxygen was used to produce a spatial distribution of dissolved oxygen. A light plane was generated across the tank by the refraction of a laser light beam, and two-dimensional images were continuously acquired with an intensified charge coupled-device (ICCD) camera. Analysis of these images revealed the sinking of cooled water to transport oxygen, and the experiments enabled the quantification of the oxygen transferred from the air into water at a range of heat fluxes. The results confirm that vertical penetration of cold-dense water can be a significant source of oxygen for lakes and reservoirs.

“Oxygen is the most fundamental parameter of lakes, aside from water itself. . .” (Wetzel 1975), and an improved understanding of water quality issues is dependent on understanding how dissolved oxygen (DO) enters and is distributed through these systems. Oxygen and other gases enter and leave a water body across the air–water interface. The rate at which this occurs is frequently parameterized as being a function of the wind speed across the surface and on the gas concentration in the water, relative to its saturation level (Broecker et al. 1978; O’Connor 1983). At times of high wind speed and low DO concentration, the transfer rate into the aqueous phase will be relatively high.

The study of gas transfer across an air–water interface has generally been conducted with reference to the ocean (for example, Watson et al. 1991; Wanninkhof 1992). Here, sus-

tained high wind speeds and deep, well-mixed surface layers are the norm. Under these conditions, shear (i.e., wind) driven transfers dominate (Brainerd and Gregg 1993). Lakes, by contrast, are often topographically sheltered, affording them protection against strong winds, and their smaller fetch lengths lead to reduced wave generation compared to the ocean (for example, Wanninkhof et al. 1985). Under these conditions, the application of oceanographically derived formulations for oxygen transfer with dependence on wind speed may be questionable.

The problem is compounded if one considers the diurnal variations of DO concentration and temperature in lakes. During the day oxygen addition to the surface water by photosynthetic production can yield high dissolved oxygen concentrations, at times exceeding the saturation concentration (Melak and Kilham 1974; Oldham and Imberger 1995). In addition, the higher surface temperature lowers oxygen solubility. An increase in water temperature from 15°C to 25°C results in an 18% decrease in oxygen solubility (Benson and Krause 1984). Therefore, during the day the DO deficit at the surface is likely to be at its lowest (possibly even absent) and oxygen transfer into the lake will be reduced.

Wind speed and surface heat flux also display a pronounced diurnal pattern, with inland lakes often having very low wind speeds at night. As the surface layer is frequently deepest and coolest at night, the oxygen deficit is at a maximum, making the potential for oxygen transfer greatest. The

¹ Present address: Department of Environmental Geosciences, Pukyong National University, 599-1 Daeyondong, Namgu, Pusan 608-737, Korea.

Acknowledgments

This research has been supported by a grant from the U.S. Environmental Protection Agency’s Science to Achieve Results (STAR) program through grant GR825428-01-0. The research described has not been subjected to any EPA review and therefore does not necessarily reflect the views of the Agency, and no official endorsement should be inferred. We thank Ian Kennedy for illuminating discussions at the inception of this work, and anonymous reviewers for constructive suggestions.

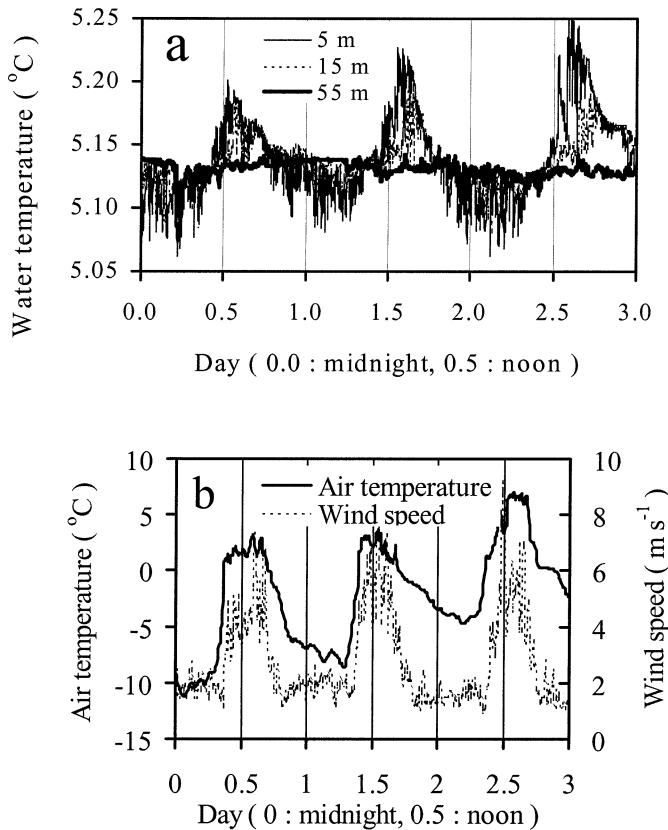


Fig. 1. Lake Tahoe data commencing midnight 25 February 1998. (a) Three day water temperature record from depths of 5, 15, and 55 m at the midlake station. (b) Wind speed and air temperature data for the corresponding period from 2 m above surface of Lake Tahoe, measured at the U.S. Coast Guard pier.

absence of solar radiation and cooler air temperatures generally results in net cooling of the water surface at night, the condition needed for natural (or penetrative) convection to occur. This is illustrated by data from Lake Tahoe, California, USA (39°N, 120°W). Figure 1a shows thermistor traces from three temperature loggers located at depths of 5, 15, and 55 m below the surface over a 3-d period, commencing at midnight on 25 February 1998. The sampling period of the temperature loggers (OEI, Model 9311) was 2 min, and the accuracy was 0.003°C. Figure 1b shows the wind speed and the air temperature for the corresponding period. The wind speed and the air temperature show a typical diurnal pattern. During each day the surface water restratified, indicating a net inward heat flux that compensated for the mixing energy of the wind. However, at night, the wind and air temperature dropped; the temperature of the surface water decreased rapidly and became lower than that of the 55-m depth, suggesting that there was active vertical mixing by natural convection.

These diurnal patterns are common in lakes and raise the question of how and when atmospheric oxygen actually enters a lake. Is it solely restricted to the coincidence of high wind and low oxygen concentration, or are there other mechanisms that may become important when these conditions do not prevail for extended periods of time? The times of

most favorable concentration gradients for the inward transfer of oxygen are at night, when the surface mixing is dominated by natural convection and wind may be totally absent. Existing models make no provision for dissolved oxygen transfer under such mixing regimes, with virtually all models possessing a strong dependence on wind speed.

Convective instabilities have been observed in the laboratory (Katsaros et al. 1977), in lakes (Imberger 1985; Brubaker 1987), and in the ocean (Shay and Gregg 1986); however, to date there have been no field, laboratory or numerical experiments conducted to look at gas exchange under such conditions.

The present work describes and quantifies the oxygen transfer associated with natural convection. To accomplish this, a laboratory experimental facility was constructed in which the destabilizing convective conditions that occur in lakes at night or throughout winter could be reproduced. The two-dimensional visualization of the convection and the quantification of the associated oxygen transport were achieved using a fluorescence technique. Laser induced fluorescence has been an active research area for a diverse range of goals (*see* for example, Lakowics et al. 1992; Wolff and Hanratty 1994; Cowen et al. 2001), and commercial sensors based on the use of fluorescence do exist. However, the use of fluorescence properties to spatially quantify and visualize the oxygen transfer is novel.

Air–water exchange models

The transfer of a gas across the air–water interface is commonly represented as

$$N = K_L(C_s - C_b) \quad (1)$$

where N is the gas flux, K_L is the mass transfer coefficient (or transfer velocity), and C_s and C_b are the concentrations of the gas at equilibrium (or saturation) and in the bulk liquid, respectively. While C_s and C_b can readily be measured, K_L must be modeled. There has been a clear departure from the earlier film models (Whitman 1923) and surface renewal models (Higbie 1935; Danckwerts 1951) toward models that incorporate the hydrodynamic features of the flows. These too have evolved in complexity, from the large eddy model (Fortescue and Pearson 1967), where the hydrodynamics were embodied in a single eddy length and time scale, to the multiscale approach embodied in eddy diffusivity models (Ueda et al. 1977; Kitaigorodskii and Donelan 1984). A number of reviews (Brtko and Kabel 1978; Theofanous 1984; Brumley and Jirka 1988) have tracked the evolution of such models.

Many of these models attempt to define common turbulent length and velocity scales over the whole range of flows (Brumley and Jirka 1988). In reality, however, the character of turbulence differs depending on the mode of turbulence generation. Hence, they suggested that each type of flow should be considered separately. To date, virtually all models that embody hydrodynamic features assume turbulence generation by mechanical shear. Laboratory experiments using grid stirring (Fortescue and Pearson 1967; Brumley and Jirka 1987; Jirka and Ho 1990) or wind tunnels (Liss 1973) have also investigated this mode. A departure from this was the

work of Soloviev and Schlüssel (1994) who, in attempting to model gas transfer over a wide range of wind speeds, have included convective effects. However, their formulation is directed at oceanic conditions ("calm" is defined as wind speeds less than 5 m s^{-1}) and still assumes an externally imposed velocity.

Natural convection

The system considered here falls between the two extremes of the Rayleigh–Taylor problem and the Bénard–Rayleigh problem. The former is characterized by two semi-infinite layers, the upper of higher density and the two being separated by a sharp interface. The latter problem is characterized by a broad region of unstable density gradient, confined above and below. There is a large body of literature describing these flows and the wide range of flows that fall between them. Turner (1979) provides an excellent summary.

The Rayleigh and the Prandtl numbers are the most important parameters describing convective flows (Turner 1979). For the Bénard–Rayleigh configuration, they may be defined as

$$\text{Ra} = \frac{g\alpha\Delta Td^3}{\kappa\nu} \quad \text{and} \quad (2)$$

$$\text{Pr} = \frac{\nu}{\kappa} \quad (3)$$

where α is the coefficient of thermal expansion, ΔT is the temperature difference between the upper and lower boundaries separated by a distance d , κ is the thermal diffusivity, ν is the kinematic viscosity, and g is the gravitational acceleration. The various forms of convection observed in a horizontal fluid layer are a function of both the Rayleigh and Prandtl numbers (Krishnamurti 1970). Below the critical value of $\text{Ra}_c = 27\pi^4/4$ there is no motion; however, for water ($\text{Pr} = 7$) the flow changes from a steady two-dimensional flow ("rolls") to a time-dependent three-dimensional flow, and ultimately to a fully turbulent flow at $\text{Ra} > 14,000 \text{ Pr}^{0.6}$, or 5×10^4 for water (Rossby 1969). The laboratory facility described below has been designed to produce fully turbulent flows with Ra up to 10^{10} , well beyond the turbulent threshold and approaching the conditions experienced in nature. Lakes would typically have Rayleigh numbers in the range of 10^{11} – 10^{12} .

Experimental methods

Fluorescence background—Fluorescent oxygen visualization (FOV) was used to quantify the amount of oxygen transferred from the air into water and to visualize the movement of the oxygen enriched water. The primary concept of FOV is based on the quenching of fluorescence intensity by oxygen. The fluorescent dye used was pyrenebutyric acid (PBA), chosen due to its fluorescence lifetime, quenching rate by oxygen, and excitation and emission wavelengths of fluorescence (Lee and Schladow 2000). Vaughan and Weber (1970) provide a detailed study of the fluorescent properties

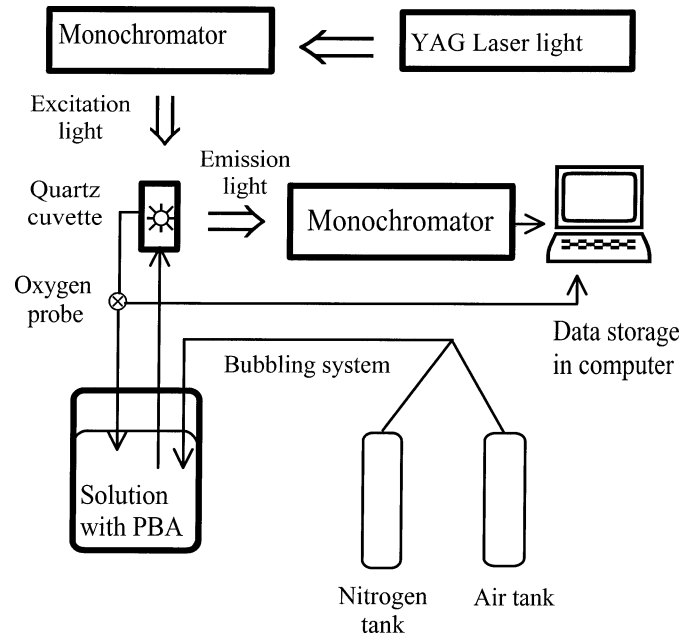


Fig. 2. Schematic of the calibration apparatus.

of PBA. The Stern–Volmer equation represents the relationship among fluorescent lifetime (f), fluorescent light intensity (F), and oxygen concentration (C):

$$\frac{f_0}{f} = \frac{F_0}{F} = 1 + KC \quad (4)$$

where the subscript 0 is the value in the absence of oxygen and K is the quenching rate constant. The PBA in the solution starts to fluoresce when a laser light at the excitation wavelength passes through the solution. The presence of oxygen in the solution quenches the fluorescence of PBA and decreases its lifetime. The fluorescent light intensity decrease correlates directly to the amount of oxygen and thus the spatial variation of the light intensity can be used to determine the distribution of oxygen concentration in the solution.

Response of fluorescent light intensity to oxygen concentration—A fluorophore for quantifying the oxygen concentration in the water should have a sufficiently large oxygen quenching yield factor to make it sensitive to oxygen concentration variations, and it should display no hysteresis in its light intensity response to oxygen concentration. The behavior of PBA fluorescence in response to oxygen concentration was determined with a specially constructed chamber (Fig. 2).

A 0.1 M stock solution of PBA (from Aldrich Chemical Company) in dimethylformamide was prepared and diluted to $3.0 \times 10^{-6} \text{ mole L}^{-1}$ in deionized water (Vaughan and Weber 1970). Solution from a 1,000-ml flask was pumped through a quartz cuvette ($1 \text{ cm} \times 1 \text{ cm} \times 3 \text{ cm}$) and was excited with a beam from a pulsed yttrium aluminum garnate (YAG) laser with a 266-nm incident wavelength. The incident energy was about 1 mJ in a 10-ns pulse. The emitted light, with a 340-nm wavelength, was focused into a monochromator, and the fluorescence intensity was continuously

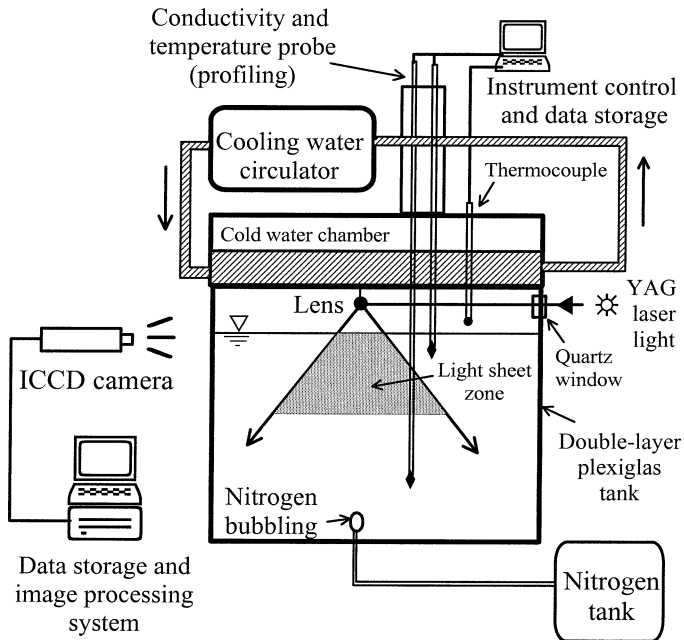


Fig. 3. Schematic of the experimental tank.

recorded as voltage values. The voltage values were normalized against the measured voltage of the incident beam intensity, thereby eliminating errors due to fluctuations in the incident beam intensity. A variable mixture of nitrogen and air was bubbled through the solution in the flask to change the oxygen concentration of the solution. The oxygen concentration was measured continuously by a YSI oxygen probe that was calibrated using a Winkler titration method (Fritz and Schenk 1974).

Tank experiment for two-dimensional visualization of oxygen concentration variation—To simulate the air–water interface in a lake subject to pure natural convection, a $0.76 \text{ m} \times 0.76 \text{ m} \times 0.6 \text{ m}$ (inner size) rectangular tank was used. The walls of the tank were constructed entirely of 1.5-cm thick Plexiglas to allow full visual access. The Plexiglas walls and base were double glazed to provide the necessary thermal insulation, with the panels separated by a 1-cm air gap. A quartz window (3 cm in diameter and 1 cm in thickness) was installed on one side wall of the tank above the air–water interface to allow the laser beam to enter the tank. The tank was filled with deionized water, and 0.1 M PBA stock solution was added to make $3.0 \times 10^{-6} \text{ mole L}^{-1}$ of PBA solution in the tank. The upper portion of the tank comprised a Plexiglas lid chamber with a 0.5-cm thick aluminum plate forming the base of the chamber. Cold water would be pumped through the lid chamber to provide a constant temperature upper boundary condition that simulated the conditions necessary for natural convection. Crushed ice and dry ice packed into the lid chamber were also used to extend the experimental range. Three ducts (1 cm in diameter) were placed in the lid to allow for exchange of gases and to provide access for temperature and conductivity probes. There was 3-cm thickness of air space between the

surface of solution and the bottom of the chamber. A schematic of the tank is shown in Fig. 3.

Prior to each experiment, the solution in the tank was bubbled with pure nitrogen for 6 h to purge oxygen from the solution. After the nitrogen bubbling was stopped, the tank was kept stable without any disturbance for 1 h to create a near-quiet initial condition for the experiment. The head space between the surface of the solution and the bottom of the lid chamber was replaced with room air at a velocity of approximately 10 cm s^{-1} , an order of magnitude lower than that required to initiate ripples on water surfaces in general (Van Dorn 1953; Miles 1962; Kahma and Donelan 1988), and in particular for the given tank “fetch length” (Caulliez et al. 1998). This precaution was necessary to avoid reintroduction of oxygen prior to commencement of the experiment.

An experiment was initiated with the cooling of the aluminum plate that formed the base of the lid chamber. Either chilled water (5°C or 12°C) was circulated through the chamber with constant flow rate or the lid chamber was packed with ice or dry ice. The initial temperature of water in the tank and the overlying air was typically 21°C , and the air temperature decreased to a stable value (8°C and 14°C for the cases of the chilled water circulation; 3°C and -3°C for the cases of ice and dry ice) within 10 min. While surface cooling in natural systems arises from a combination of factors, including radiant cooling and evaporation as well as thermal conduction, the experiments relied almost solely on thermal conduction. However, since the heat fluxes produced were of a similar magnitude to those that could be experienced in nature, the source of the cooling was not an issue.

For imaging experiments, a YAG laser with 266-nm laser pulse was used to excite the PBA that was dissolved in the water of the tank. The pulse frequency of the YAG laser was 20 Hz. As with the calibration, the voltage values were normalized against the measured voltage of the incident beam intensity. The laser beam was focused onto a cylindrical lens that expanded light into a planar sheet of 1-mm thickness. The two-dimensional light intensity field produced by the light sheet was recorded on an intensified charge coupled-device (ICCD) camera oriented at 90° to the light sheet. Images were recorded every 5 s for 3 h, this frequency being dictated by the time needed to store each image. A black and white ICCD camera with 577×384 pixels (Princeton Instruments, model: ICCD-576G) was used with a 50-ns exposure time. Each image covered an area of $10 \text{ cm} \times 8 \text{ cm}$ at the center of the tank, just below the water surface. Images were stored on a computer hard drive and processed after the experiment using image processing software (WinView, Princeton Instruments). Each image was also transferred to an 8 bit grayscale (0 to 255 integer value) TIF image file, each file about 50 kB in size for further visualization analysis.

Calibration of ICCD camera response to oxygen concentration—The detection systems of the ICCD camera were calibrated with the laser light emission from PBA solutions with different DO concentrations. Six rectangular quartz tubes ($1 \text{ cm} \times 1 \text{ cm} \times 3 \text{ cm}$) were filled with a known PBA solution, each with a different DO concentration in the range

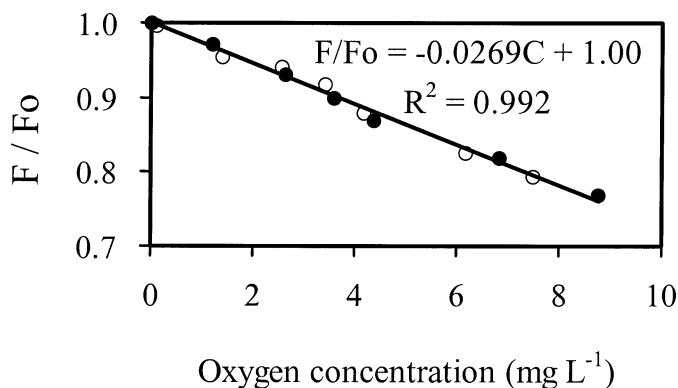


Fig. 4. The calibration of light intensity versus oxygen concentration at 21°C. Filled circles represent the values while the oxygen concentration was decreasing. Open circles represent the values while the oxygen concentration was increasing.

of 0.0 to 9.0 mg L⁻¹. The average light intensity in 10 pixels at the center of the image of the tubes was used for the calibration of the intensity versus oxygen concentration. Calibrated fluorescence intensity curves were used to convert the image intensity to time-resolved oxygen concentration profiles. The relationship of the intensity of PBA solution to temperature has been described in Lee and Schladow (2000). The sensitivity of fluorescence intensity to temperature is small (less than 10% change over a temperature range of 35°C). The temperature effect on the fluorescence intensity was therefore neglected in all the experiments.

High-resolution profiles for temperature and electrical conductivity—High-resolution profiles of temperature and electrical conductivity were used to define the temperature structure induced by the surface cooling. A microscale conductivity–temperature instrument (Precision Measurement Engineering) that comprised a four-electrode conductivity probe and a thermistor assembly was used (Head 1983). The conductivity sensor provided a good measure of the boundary between air and water, and the thermistor provided a direct measure of temperature as the fundamental variable of convective instability. The spatial resolution of the profiles was about 0.1 mm. The conductivity probe had a time constant of 0.004 s and a resolution of 2.5 μS m⁻¹. The thermistor had a time constant of 0.012 s and resolution of 0.005°C (Head 1983). A stepper motor, controller, and lead screw were used to drive the probe vertically. Another thermistor was located at a fixed depth in the tank, and one thermocouple was located above the water surface to measure the temperature of overlying air continuously.

Results and discussion

Response of fluorescence to oxygen concentration—Figure 4 shows the response curve of the light intensity measured by a monochromator versus oxygen concentration in the PBA solution. The solution in the flask was bubbled with nitrogen to expel oxygen for 30 min. The oxygen concentration of the solution was increased from 0.1 mg L⁻¹ to 8.7 mg L⁻¹ by bubbling air through the solution while the light

intensity was recorded continuously. The experiment was repeated while decreasing oxygen concentration by bubbling nitrogen to verify that there was no hysteresis of the calibration curve. The total fluorescent yield of PBA solution was decreased by a factor of 0.77 over the range tested, a 23% decrease in intensity due to oxygen quenching. The entire test (increasing and then decreasing oxygen) was repeated 10 times. The difference in the linear calibrations generated was less than 0.1 mg L⁻¹ or 1%. This was attributed to the fluctuations in the incident laser power, despite normalization. Several other fluorophores were tested, including Rhodamine-WT, Keton red-WT, tetra bromorhodamine 123 bromide, biacetyl (2,3-butanedione), and tris (2,2'-bipyridine) ruthenium (II) chloride. Of these, PBA gave the greatest dynamic response for the range of oxygen concentrations tested. No hysteresis was observed when the experiments were performed with the room lights off. When the room lights were on, the fluorophore appeared to saturate over time, leading to hysteresis. Short timescale (millisecond) photobleaching of the type described by Saylor (1995) was also not detected, possibly because of the extremely short (10 ns) laser pulse length. On balance, these results suggest that with simple precautions PBA could be used to quantify the dissolved oxygen concentration.

Preprocessing of images for oxygen concentration distribution—Several steps were necessary to obtain accurate two-dimensional visualization of the dissolved oxygen concentration. These are described below.

Normalization of planar light field—The planar light intensity field produced by a cylindrical glass lens was not homogeneous. In the horizontal direction, the central portion of the light sheet was brighter than the edge portion. The inhomogeneity was due to the Gaussian distribution profile of the laser beam. To compensate for this, the horizontal, nonuniform light field was normalized by a third-order polynomial fitting method (Krauss et al. 1995), such that

$$X = ax^3 + bx^2 + cx + d \quad (5)$$

where X is the normalized factor, x is the distance from the edge of the image, $a = -2.27 \times 10^{-5}$, $b = 0.738$, $c = -0.015$, and $d = 101.484$. In the vertical direction, the light field was inhomogeneous due to the progressive attenuation of light through the water column. Light attenuation by the water in the tank is governed by Lambert-Beer's law and is an exponential function of the concentration of absorbing substance present (PBA) and the sample path length (Wayne 1988). The absorptivity of PBA solution was measured using an ultraviolet spectrometer (Perkin-Elmer lambda one), and the normalization of vertical light intensity in the image was performed by an exponential fitting curve. The refraction and reflection of light by the walls and laser light scattering may also affect the nonuniformity of light intensity in the image. To minimize the impact of reflection and wall effects, it was necessary to minimize the area of the image but maintain a size large enough to evaluate the oxygen transfer at the interface. An area 5-cm wide × 3-cm deep, (350 × 200 pixels) was used in the final two-dimensional image processing. The full number of available pixels was not used to

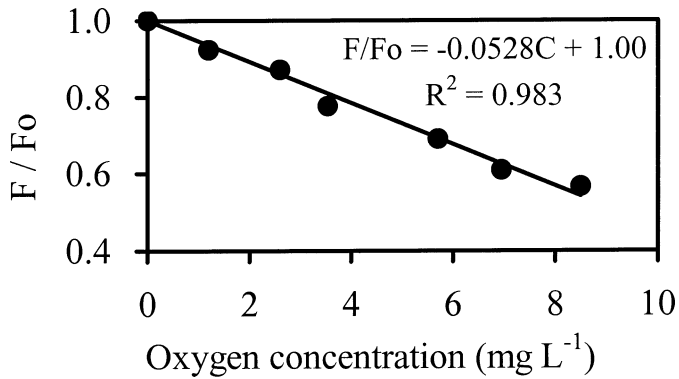


Fig. 5. Calibration line of light intensity versus oxygen concentration in the image acquired from ICCD camera at 21°C.

eliminate the possible effect of vignetting (Cowen et al. 2001).

Calibration curve of intensity versus oxygen concentration—Figure 5 shows a calibration curve of light intensity to the oxygen concentration variation in the ICCD camera image. Such curves were generated immediately before and after each experiment (as tank water was sometimes changed between experiments), and the results averaged to produce a unique equation for each experiment. Typically the standard deviation for each curve fit was less than 0.5% in concentration. About 43% of intensity decreased in a range from 0.0 mg L⁻¹ to 8.5 mg L⁻¹. The observed quenching, derived from the Stern–Volmer plot from the ICCD data (Fig. 5), was larger than that from the monochromator (Fig. 4), since the ICCD camera accepted the emitted light of PBA in a wider wavelength range than the monochromator. The quenching rate constant, (K), from Eq. 4 is given by the slopes of these curves and is typically -0.0269 for the monochromator (Fig. 4) and -0.0528 for the ICCD camera (Fig. 5). The calibration curves were directly used to recreate the oxygen concentration image from the light intensity image.

The two-dimensional image of oxygen concentration distribution—Sequential images of oxygen concentration variation were produced from the image processing. A total of 2,160 images were processed for each 3-h experiment. Figure 6 illustrates the transfer of dissolved oxygen caused by the convectively unstable conditions. Each panel shows the oxygen concentration variation at four times during a 1-min interval. The white background represents an ambient concentration of 0.08 mg L⁻¹ of oxygen, which was the measured initial condition. The shades of gray represent progressively higher oxygen concentrations. Absolute accuracy of the oxygen measurements is better than 0.1 mg L⁻¹ of oxygen, while resolution is approximately 0.03 mg L⁻¹. For clarity, the dissolved oxygen field is displayed in four concentration bands, although the data showed up to 256 discrete levels. The multitude of gray tones when displaying all the variations tended to blur the essential pattern. The concentration near the surface exceeded 6.5 mg L⁻¹.

The oxygen-rich plumes have their origin in the thermal

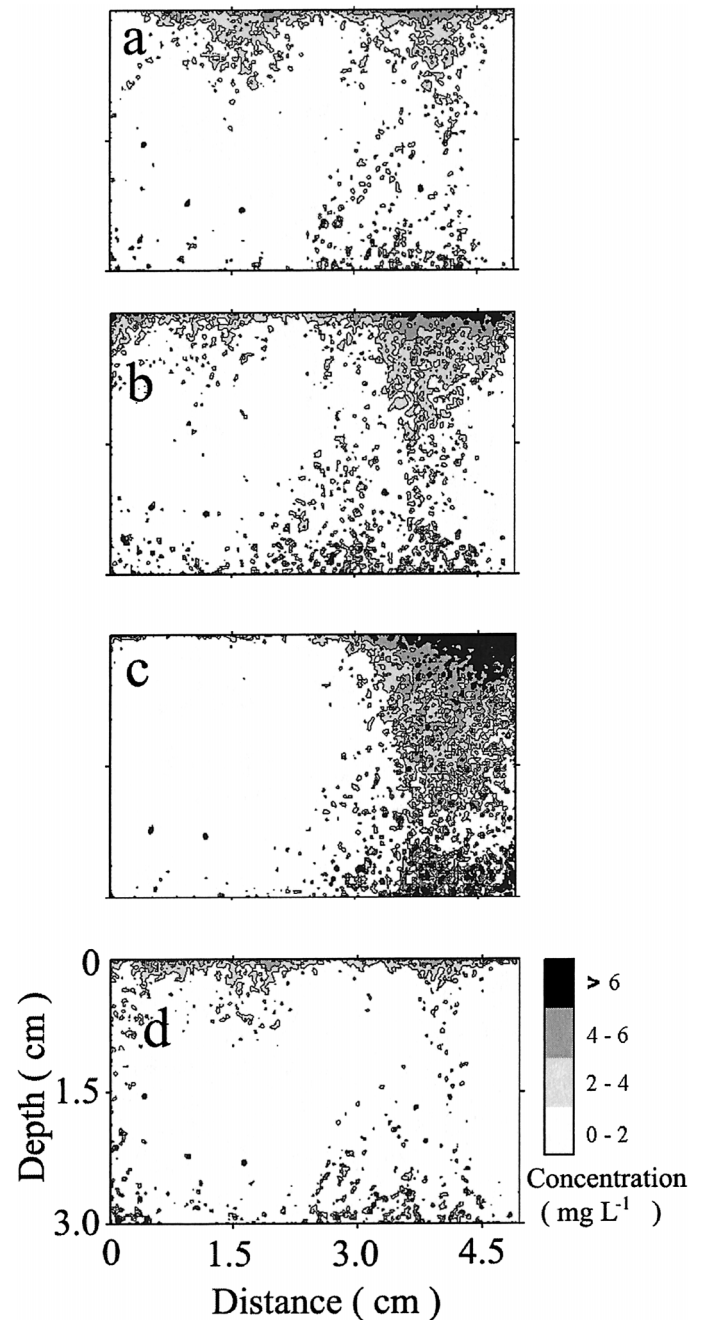


Fig. 6. Oxygen concentration distribution during a convective plume event: (a) after 30 min 00 s of cooling, (b) after 30 min 10 s of cooling, (c) after 30 min 30 s of cooling, (d) after 31 min 00 s of cooling.

boundary layer. The thickness of the thermal boundary layer was in the range of 2 to 4 mm (Fig. 6 and Fig. 8a). This layer thickened in localized areas as parcels of cold, oxygen-rich water accumulated before being shed and transferred downward. This cycle of plume penetration was repeated many times during an experiment. The time for one cycle was variable, but in a range from 20 to 60 s. Figure 7 illustrates the plume penetration over a 20-min period, demonstrating that the cold water carrying oxygen was plunging

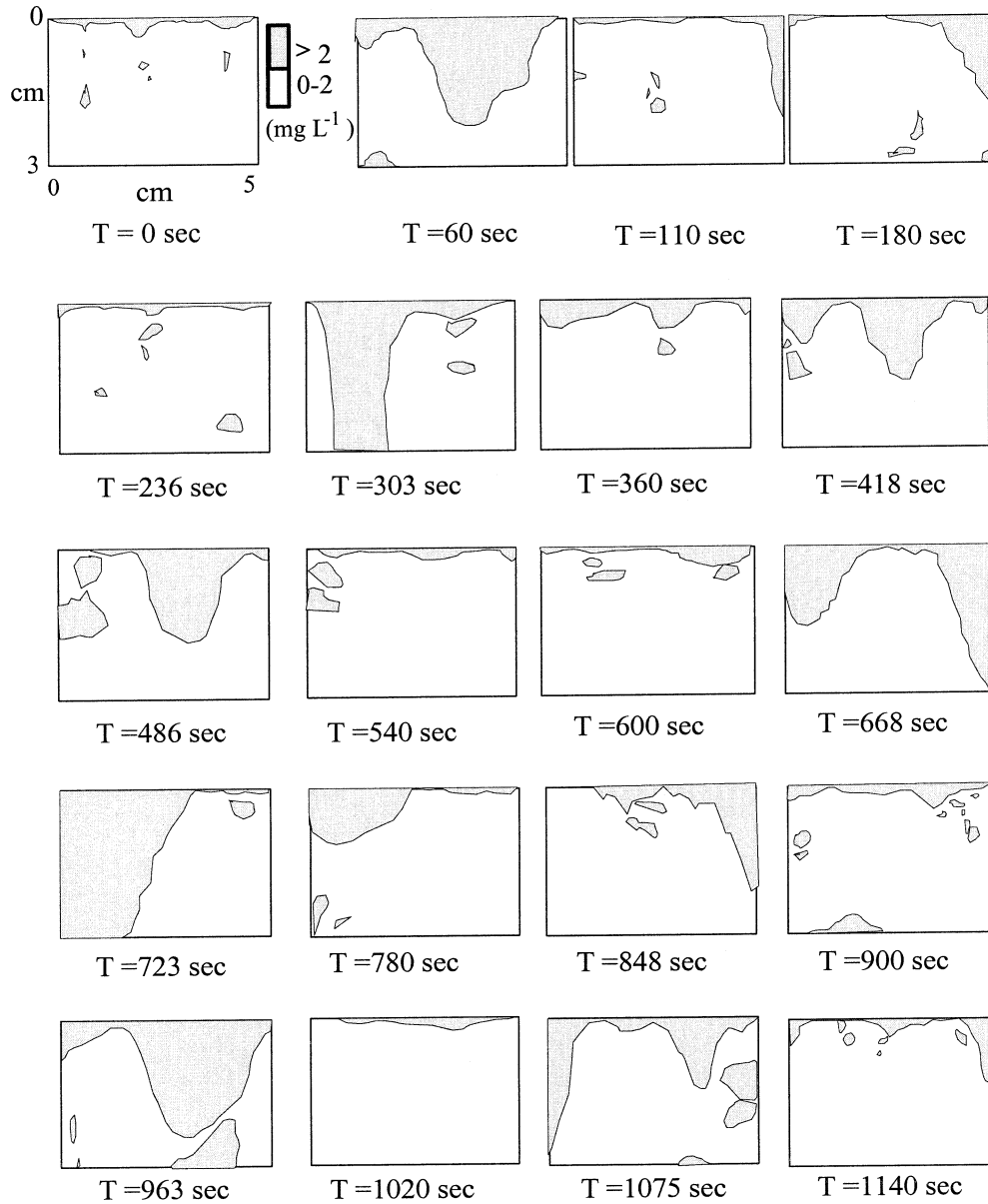


Fig. 7. Visualization of oxygen plume penetration demonstrating spatial and temporal variability during 20 min. Individual panels are at approximately 1-min intervals.

down to a lower part of the tank during the cooling experiment. The locations of these thickening regions were constantly changing and appeared to be randomly distributed. The concentrations are shown in just two bands to highlight the changes in the spatial and temporal distribution.

High-resolution profiles of temperature—High-resolution temperature and electrical conductivity profiles were taken at a fixed location at either 5 or 10-min intervals during each experiment. The electrical conductivity profile was used to identify the exact position of the air–water interface in the profiles, as a discontinuity in conductivity occurred at the interface. By contrast the temperature profile was continuous through the interface. Figure 8a shows five vertical thermal profiles within 12 mm of the air–water interface. The profiles

were taken 30 min after the commencement of the experiment and at 5-min intervals thereafter. A constant surface temperature of approximately 8°C was maintained through this experiment. The initial temperature of the tank water was 21°C. Heat loss by thermal conduction dominated the thermal exchange at the surface of the tank. As the temperature in the tank decreased through the experiment, the heat flux was not constant; however, the departure from a constant heat flux was small (<1%) over the 30-min period shown. Heat flux (H) by thermal conductivity in the experiment could be calculated from the temperature difference across the aluminum base plate in the tank lid, such that

$$H = -k \frac{A}{L} (T_1 - T_2) \quad (6)$$

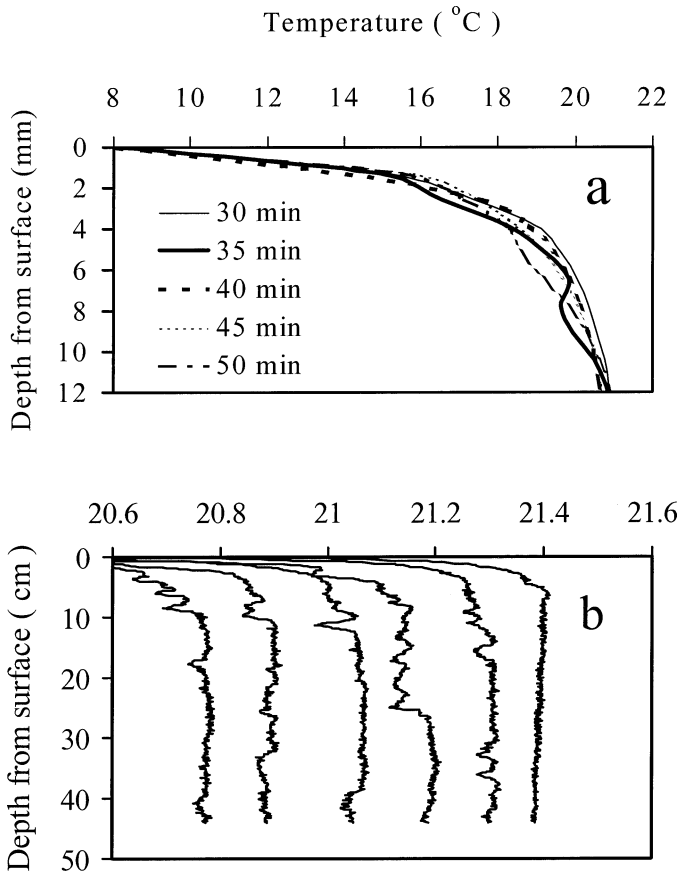


Fig. 8. (a) Temperature profiles in upper 12 mm, 30 min after commencement of an experiment and at 5-min intervals thereafter. (b) Vertical temperature profiles over the full depth of the tank during one experiment. Profiles start from the right at $t = 30$ min and are shown at 30-min intervals for a 3-h experiment.

where A is the area normal to the flux direction, k is the thermal conductivity of the medium (aluminum of the top lid in tank: $237 \text{ W m}^{-1} \text{ K}^{-1}$), L is the thickness of the medium (0.005 m), and T is the temperature at the surfaces. The calculated heat fluxes in the experiments are shown in Table 1.

The shapes of the temperature profiles near the interface are similar to the ones observed by Katsaros et al. (1977). The profiles tend to overlap each other, with the exception of time varying deviations in each profile. The deviations in the temperature profiles represent different stages in the localized thickening of the thermal source layer. What was previously referred to as the thermal boundary layer, where most of the temperature change occurs, is within 2–4 mm of the boundary.

Figure 8b shows a set of temperature profiles over the full depth of the tank. The profiles shown are at 30-min intervals, commencing 30 min after the start of a 3-h experiment. What is evident in these profiles is that the transport produced by the convective plumes extended the full depth of the tank and that the water column was maintained in a generally well-mixed state during the experiment. Clearly, if the cool water is being well distributed by the motions then the dissolved oxygen being carried will also be well distributed and

Table 1. The oxygen transfer coefficients and heat fluxes in the tank (temperature of water was approximately 21°C). ΔT is the temperature difference between air and water, C_s is the saturation oxygen concentration, C is the initial oxygen concentration, C_f is the final oxygen concentration, F is the oxygen flux, K_L is the oxygen transfer coefficient, and H is the heat flux.

ΔT ($^\circ\text{C}$)	7	13	18	24
C_s (mg L^{-1})	8.5	8.5	8.5	8.5
C (mg L^{-1})	0.085	0.085	0.085	0.085
C_f (mg L^{-1})	0.250	0.350	0.650	1.030
F ($\text{mg m}^{-2} \text{ day}^{-1}$)	752.0	1813.0	2576.0	4309.0
K_L (m day^{-1})	0.09	0.22	0.31	0.51
H (W m^{-2})	402.9	568.8	711.0	900.6

extend over the full depth of the tank. Despite the fact that the temperature difference between water in the thermal source layer and the ambient water was 13°C , the temperature fluctuations produced by the cold plume water in the ambient water were only 0.1°C in locations away from the interface, a reduction of 2 orders of magnitude (Fig. 8b). This suggests that there is considerable entrainment occurring as the plumes descend. Even close to the base of the thermal source layer there appears to have been considerable entrainment. The frequent occurrence of temperature gradient reversals in the profiles is a signature of active convective overturning. Temperature measured continuously at a fixed point 5 mm below the surface showed temperature fluctuations of order 1.0°C during a penetration event (Fig. 9), an order of magnitude less than the temperature difference between the ambient temperature at this depth and the surface. Such a result is consistent with the oxygen measurements in Fig. 6, where an order of magnitude reduction in DO concentration compared to saturation at the surface temperature of 8°C was observed. The penetration event lasted about 20 s, similar to the results of image analysis (Fig. 6). These results also justify the neglect of the temperature effect on PBA fluorescence, since significant temperature differences only occur within several millimeters of the surface.

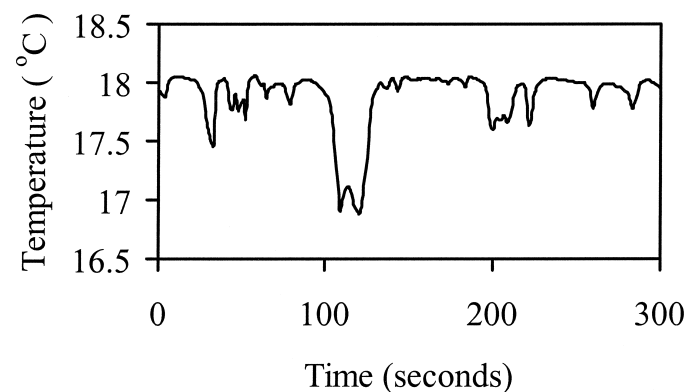


Fig. 9. Temperature variation of surface water (at 0.5-cm depth) during experiment, showing temperature of penetrating water. Sampling frequency is one sample per second.

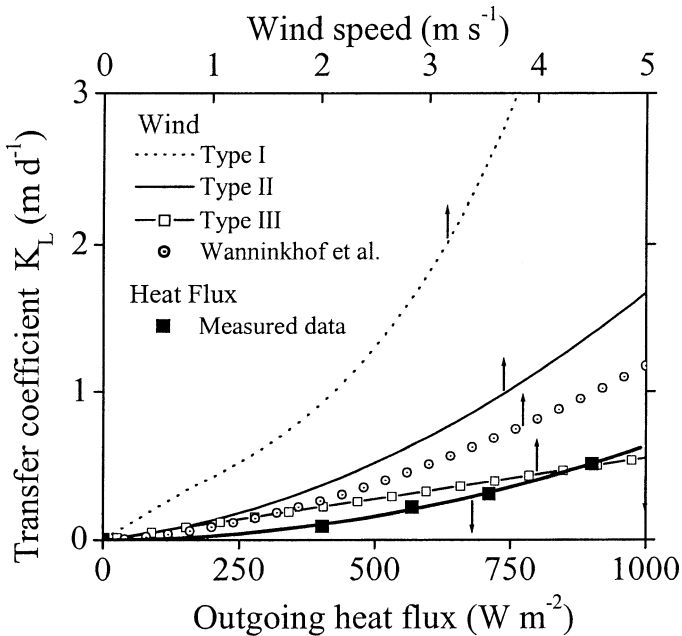


Fig. 10. Transfer coefficient as a function of outgoing heat flux from experimental results and as a function of wind speed from classification proposed by O'Connor (1983) and formulation by Wanninkhof et al. (1991).

Measurement of the oxygen transfer rate—The amount of oxygen transferred from the air to the water was measured for four values of temperature difference (heat flux). For each case, the water in the tank was bubbled with nitrogen for 5 h to extract oxygen from the water before commencement of an experiment. The dissolved oxygen concentration in the water was measured at seven different locations in the tank using a YSI oxygen probe (Model 59 dissolved oxygen meter) immediately prior to commencing surface cooling. The cooling was applied for 2 h. At the completion of the cooling phase, CO₂ gas was passed into the air space between the cooling chamber and the water surface. CO₂ is heavier than air and readily displaced the air through the vent in the top of the lid, thereby halting any further oxygen transfer. The tank was stirred with a stainless steel stir rod for 20 min and the oxygen concentration was measured at the same locations in the tank. The change in concentration when multiplied by the tank depth and divided by the duration of the experiment yielded the oxygen flux. The measured total oxygen flux for the four heat flux values is summarized in Table 1. Assuming negligible oxygen transfer (molecular diffusion) with zero heat flux, the data can be fit with the equation

$$N = 0.0055H^2 - 0.163H \quad (7)$$

where N is the dissolved oxygen flux ($\text{mg m}^{-2} \text{d}^{-1}$) and H is the heat flux out of the tank (W m^{-2}). The oxygen flux increases significantly with an increase in the outgoing heat flux. This is consistent with the results of Katsaros et al. (1997), where the frequency of plume formation at the surface increases with increasing heat flux. Combining Eqs. 1 and 7, the oxygen transfer coefficients (K_L) for four different cooling rates can be calculated and the values presented in

Table 2. Measured wind speed and calculated heat flux and oxygen transfer coefficients for Lake Tahoe for the period 22 November 1998 to 22 February 1999.

	Heat flux (W m^{-2})	Wind speed (m s^{-1})	$K_{L\text{heat flux}}$ (m d^{-1})	$K_{L\text{wind}}$ (m d^{-1})
Maximum	-736.4	14.9	0.34	1.64
Mean	-221.5	3.64	0.037	0.4
Minimum	0	0.46	0	0.05

Table 1 and Fig. 10. These values can also be regressed with a second order polynomial to yield

$$K_L = 6.293 \times 10^{-7}H^2 + 1.036 \times 10^{-6}H \quad (8)$$

Relevance for oxygen transport in lakes—Figure 10 shows the value of K_L plotted against heat flux (the results from our experiments) and against wind speed. These latter curves are based on the classification and equations proposed by O'Connor (1983), where he distinguished between measurements that were pertinent to oceans and very large lakes (wind speeds greater than 20 m s^{-1}), those made at laboratory or small-scale field scale (wind speed less than 6 m s^{-1}) and those in between. In Fig. 10, where we reproduce the average curves he produced from a broad range of data, we denote these three regimes as type I, II, and III, ranging from the largest scales to the smallest, respectively. These curves serve to indicate the great disparity that exists in this measurement, a great part of which is due to the very different condition under which experiments were performed. In addition, we plot the relationship derived by Wanninkhof et al. (1991) for gas transfer in lakes. If we assume that the type II or type III curves apply for wind-driven oxygen transport for lakes that are topographically sheltered or of limited fetch, then the transfer coefficient associated with natural convection is always smaller for the range of variables shown. However, this transfer coefficient is by no means negligible. Using Lake Tahoe as an example (which, with a surface area of 501 km^2 is barely a fetch limited and topographically sheltered lake), one can calculate the two transfer coefficients. Table 2 shows the wind and net heat flux, as well as the respective oxygen transfer coefficients. The heat flux was calculated (see TVA 1972) using hourly averaged data and then averaged for the period 22 November 1998 to 22 February 1999. The measured meteorological parameters used to calculate the heat flux are the wind speed, air temperature, relative humidity, longwave radiation, and shortwave radiation. Although it is clear that the uncertainty in all the wind based data is high, it can be said that natural convection can have a major impact on oxygen transfer. Over the winter period the value of the convection-driven oxygen transfer coefficient is approximately 9% of the wind-driven oxygen transfer coefficient. However, on individual days the fraction can rise to as much as 40%. Further, this only partly reflects the effect on oxygen transfer. As discussed previously, the mass of oxygen transfer also depends on the concentration difference, as given by Eq. 1.

Oxygen transfer associated with natural convection in lakes and reservoirs was examined in a series of laboratory

experiments. A thin, cool surface water layer (2–3 mm in thickness) was formed by chilling the overlying air. The surface water layer became gravitationally unstable, resulting in the formation of negatively buoyant thermal plumes, which penetrated through the total depth of the water column. A fluorescent oxygen visualization (FOV) technique was developed to quantitatively view the oxygen transfer at the air–water interface. DO distribution at the air–water interface was continuously visualized to provide the evidence of the vertical sinking of cold water driving oxygen transport. The technique provided a phenomenological description of plumes under a cooling water surface and the mechanism of oxygen transfer under a physically realizable, ubiquitous set of natural conditions in the lakes. The oxygen transfer coefficients and oxygen fluxes produced by the natural convection were measured at four near-constant heat fluxes. For the range of temperature differences 7°C – 24°C (the range of heat fluxes 403 – 901 W m^{-2}), the oxygen transfer coefficients (K_L) were in the range of 0.09 – 0.51 m d^{-1} and the total oxygen fluxes (F) were between 752 and $4,309\text{ mg m}^{-2}\text{ d}^{-1}$. The deep penetration of cooling water was also observed from the temperature profiling in the tank, and it was determined to be a significant oxygen source to the deeper parts of a lake.

These experiments have gone part way to removing the uncertainty associated with natural convection as a source of oxygen. Calculated oxygen transfer at Lake Tahoe was seen to be a small, but not insignificant, contributor to the seasonal oxygen budget. On shorter time scales, as might apply over a field experiment, the role of natural convection could be more important, depending on the conditions. It is likely that in systems that are more wind sheltered than Tahoe, for example flood mine pits (Stevens and Lawrence 1998) or deeply incised dendritic reservoirs, that this mechanism may be even more important.

References

- BENSON, B. B., AND D. KRAUSE, JR. 1984. The concentration and isotopic fractionation of oxygen dissolved in fresh water and seawater in equilibrium with the atmosphere: I. Oxygen. *Limnol. Oceanogr.* **29**: 620.
- BRAINERD, K. E., AND M. C. GREGG. 1993. Diurnal restratification and turbulence in the oceanic surface mixed layer—part I: Observations. *J. Geophys. Res.* **98**: 22645–22656.
- BROECKER, H. C., J. PETERMANN, AND W. SIEMS. 1978. The influence of wind on CO_2 exchange in a wind-wave tunnel. *J. Mar. Res.* **36**: 595.
- BRTKO, W. J., AND KABEL, R. L. 1978. Transfer of gases at natural air–water surfaces. *J. Phys. Oceanogr.* **8**: 543–556.
- BRUBAKER, J. M. 1987. Similarity structure in the convective boundary layer of a lake. *Nature* **330**: 742–745.
- BRUMLEY, B. H., AND G. H. JIRKA. 1987. Near-surface turbulence in a grid-stirred tank. *J. Fluid Mech.* **183**: 235–263.
- , AND ———. 1988. Air–water transfer of slightly soluble gases: Turbulence, interfacial processes and conceptual models. *Physicochemical Hydrodynamics* **10**: 295–319.
- CAULLIEZ, G., N. RICCI, AND R. DUPONT. 1998. The generation of the first visible wind waves. *Phys. Fluids* **10**: 757–759.
- COWEN, E. A., K.-A. CHANG, AND Q. LIAO. 2001. A single-camera coupled PTV-LIF technique. *Exp. Fluids* **31**: 63–73.
- DANCKWERTS, P. V. 1951. Significance of liquid-film coefficients in gas absorption. *Ind. Eng. Chem.* **43**: 1460–1467.
- FORTESCUE, G. E., AND J. R. A. PEARSON. 1967. On gas absorption into a turbulent liquid. *Chem. Eng. Sci.* **22**: 1163–1175.
- FRITZ, J. S., AND G. H. SCHENK, JR. 1974. Quantitative analytical chemistry, 3rd ed. Allyn and Bacon.
- HEAD, M. J. 1983. The use of miniature four-electrode conductivity probes for high resolution measurement of turbulent density or temperature variations in salt-stratified water flows, Ph.D. dissertation. Univ. of California, San Diego.
- HIGBIE, R. 1935. The rate of absorption of a pure gas into a still liquid during short periods of exposure. *AIChE. Trans.* **31**: 365–388.
- IMBERGER, J. 1985. The diurnal mixed layer. *Limnol. Oceanogr.* **30**: 737–770.
- JIRKA, G. H., AND A. H. W. HO. 1990. Measurements of gas concentration fluctuations at water surface. *J. Hydraul. Eng.* **116**: 835–847.
- KAHMA, K. K., AND M. A. DONELAN. 1988. A laboratory study of the minimum wind speed for wind wave generation. *J. Fluid Mech.* **192**: 339–364.
- KATSAROS, K. B., W. T. LIU, J. A. BUSINGER, AND J. E. TILLMAN. 1977. Heat transfer and thermal structure in the interfacial boundary layer measured in an open tank of water in turbulent free convection. *J. Fluid Mech.* **83**: 311–335.
- KRISHNAMURTI, R. 1970. On the transition to turbulent convection. *J. Fluid Mech.* **42**: 295–320.
- KITAIGORODSKII, S. A., AND M. A. DONELAN. 1984. Wind-wave effects on gas transfer. *In* W. Brutsaert and G. H. Jirka [eds.], *Gas transfer at air–water surfaces*. Reidel.
- KRAUSS, T. P., L. SHURE, AND J. N. LITTLE. 1995. Signal processing toolbox. The Math Works.
- LAKOWICZ, J. R., H. SZMACINSKI, K. NOWACZYK, K. W. BERNDT, AND M. JOHNSON. 1992. Fluorescence lifetime imaging. *Anal. Biochem.* **202**: 316–330.
- LEE, M., AND S. G. SCHLADOW. 2000. Visualization of oxygen concentration in water bodies using a fluorescence technique. *Water Res.* **34**: 2842–2845.
- LISS, P. S. 1973. Processes of gas exchange across an air–water interface. *Deep-Sea Res.* **20**: 221–238.
- MELAK, J. M., AND P. KILHAM. 1974. Photosynthetic rates of phytoplankton in east African alkaline, saline lakes. *Limnol. Oceanogr.* **19**: 743–755.
- MILES, J. W. 1962. On the generation of surface waves by shear flows: Part 4. *J. Fluid Mech.* **13**: 433–448.
- O’CONNOR, D. J. 1983. Wind effects on gas–liquid transfer coefficients. *J. Environ. Eng.* **109**: 731.
- OLDHAM, C., AND J. IMBERGER. 1995. Oxygen patchiness in a lake. *Aquat. Sci.* **57**: 325–337.
- ROSSBY, H. T. 1969. A study of Bénard convection with and without rotation. *J. Fluid Mech.* **36**: 309–335.
- SAYLOR, J. R. 1995. Photobleaching of disodium fluorescein in water. *Exp. Fluids* **18**: 445–447.
- SHAY, T. J., AND M. C. GREGG. 1986. *J. Phys. Oceanogr.* **16**: 1177–1198.
- SOLOVIEV, A. V., AND P. SCHLÜSSEL. 1994. Parameterization of the cool skin of the ocean and of the air–ocean gas transfer on the basis of modeling surface renewal. *J. Phys. Oceanogr.* **24**: 1339–1346.
- STEVENS, C., AND G. A. LAWRENCE. 1998. Stability and meromixis in a water-filled mine pit. *Limnol. Oceanogr.* **43**: 216–224.
- TENNESSEE VALLEY AUTHORITY (TVA). 1972. Heat and mass transfer between a water surface and the atmosphere. Water Resources Research Laboratory Report No. 14. Report No. 0-6803. Norris, Tennessee.
- THEOFANOUS, T. G. 1984. Conceptual models of gas exchange. *In*

- W. Brutsaert and G. H. Jirka [eds.], Gas transfer at air-water surfaces. Reidel.
- TURNER, J. S. 1979. Buoyancy effects in fluids. Cambridge Univ. Press.
- UEDA, H., R. MOLLER, S. KOMORI, AND T. MIZUSHINA. 1977. Eddy diffusivity near the free surface of open channel flow. *Int. J. Heat Mass Transf.* **20**: 1127.
- VAN DORN, W. G. 1953. Wind stress on an artificial pond. *J. Mar. Res.* **12**: 249–276.
- VAUGHAN, W. M., AND G. WEBER. 1970. Oxygen quenching of pyrenebutyric acid fluorescence in water. A dynamic probe of the microenvironment. *Biochem.* **9**: 464–473.
- WANNINKHOF, R. H. 1992. Relationship between windspeed and gas exchange over the ocean. *J. Geophys. Res.* **97**: 7373–7382.
- , J. R. LEDWELL, AND W. S. BROECKER. 1985. Gas exchange—wind speed relation measured with sulphur hexafluoride on a lake. *Science* **227**: 1224–1226.
- , ———, AND J. CRUSIUS. 1991. Gas transfer velocities on lakes measured with sulfur hexafluoride, p. 441–458. *In* S. C. Wilhelms and J. S. Gulliver [eds.], Air-water mass transfer. Am. Soc. Civil Engineers.
- WATSON, A. J., R. C. UPSTILL-GODDARD, AND P. S. LISS. 1991. Air-sea gas exchange in rough and stormy seas, measured by a dual tracer technique. *Nature* **349**: 145–147.
- WAYNE, R. P. 1988. Principles and applications of photochemistry. Oxford Univ. Press.
- WETZEL, R. G. 1975. *Limnology*. W.B. Saunders.
- WHITMAN, W. G. 1923. Preliminary experimental confirmation of the two-film theory of gas absorption. *Chem. Metall. Eng.* **29**: 146–148.
- WOLFF, L. M., AND T. J. HANRATTY. 1994. Instantaneous concentration profiles of oxygen accompanying absorption in a stratified flow. *Exp. Fluids* **16**: 385–392.

Received: 14 June 2001
Accepted: 19 March 2002
Amended: 31 May 2002